

INTERSTELLAR ABUNDANCES TOWARD X Per, REVISITED

LYNNE A. VALENCIC^{1,2} AND RANDALL K. SMITH³

¹ Johns Hopkins University, Baltimore, MD 21218, USA

² NASA Goddard Space Flight Center, Greenbelt, MD 20771, USA

³ Smithsonian Astrophysical Observatory, Cambridge, MA 02138, USA

Received 2012 July 20; accepted 2013 April 24; published 2013 May 20

ABSTRACT

The nearby X-ray binary X Per (HD 24534) provides a useful beacon with which to examine dust grain types and measure elemental abundances in the local interstellar medium (ISM). The absorption features of O, Fe, Mg, and Si along this line of sight were measured using spectra from the *Chandra X-Ray Observatory*'s LETG/ACIS-S and *XMM-Newton*'s RGS instruments, and the *Spex* software package. The spectra were fit with dust analogs measured in the laboratory. The O, Mg, and Si abundances were compared to those from standard references, and the O abundance was compared to that along lines of sight toward other X-ray binaries. The results are as follows. First, it was found that a combination of MgSiO₃ (enstatite) and Mg_{1.6}Fe_{0.4}SiO₄ (olivine) provided the best fit to the O K edge, with $N(\text{MgSiO}_3)/N(\text{Mg}_{1.6}\text{Fe}_{0.4}\text{SiO}_4) = 3.4$. Second, the Fe L edge could be fit with models that included metallic iron, but it was not well described by the laboratory spectra currently available. Third, the total abundances of O, Mg, and Si were in very good agreement with that of recently re-analyzed B stars, suggesting that they are good indicators of abundances in the local ISM, and the depletions were also in agreement with expected values for the diffuse ISM. Finally, the O abundances found from X-ray binary absorption spectra show a similar correlation with Galactocentric distances as seen in other objects.

Key word: ISM: abundances

Online-only material: color figures

1. INTRODUCTION

An integral part of understanding the interstellar medium (ISM) and building realistic dust grain models is determining the abundances of the elements in the dust phase. The most common method is to measure this indirectly, that is, to measure the gas-phase abundance and subtract this from the total (gas+dust) abundance. The gas-phase component of the local ISM is fairly well-known, having been determined by UV/optical absorption studies by many authors (Cardelli et al. 1996; Sofia et al. 1997, 1998; Cardelli & Meyer 1997; Jensen et al. 2005; Gnacinski & Krogulec 2006) and appears to be relatively independent of the line of sight used. However, the total local ISM elemental abundances are not well known, and proxies must be used instead.

Historically, the Sun has been used as the standard for ISM abundances. Carbonaceous chondrites, which reflect the abundances of the solar nebula, have been studied, as has the solar photosphere (Lodders 2003; Lodders et al. 2009; Asplund et al. 2009). However, while most solar abundances have remained more or less constant over the years, those of the main dust-forming elements have been revised downward considerably (Anders & Grevesse 1989; Grevesse & Sauval 1998; Asplund et al. 2005, 2009). The recent revisions have brought solar O into better agreement with inferred ISM abundances of Wilms et al. (2000) and Sofia & Meyer's (2001) young F and G stars. However, large scatter remains and there is no particularly persuasive reason why the 4.5 Gyr old Sun should be an accurate representation of the ISM today.

B stars and metal-rich F and G stars have also been suggested as proxies for the ISM but these have problems of their own. Hempel & Holweger (2003) showed that B stars cannot be considered an accurate indicator of ISM abundances, as element stratification due to diffusion appears common in these

stars. Thus the abundances measured at their surfaces do not necessarily reflect the abundances of the clouds from which they formed, though the latest revision of B star abundances seem to ease differences between them and solar values somewhat (Nieva & Simón-Díaz 2011). Regarding F and G stars, Edvardsson et al.'s (1993) study of stars in the solar neighborhood showed that there is large scatter in their age-metallicity relation; thus, metal-rich F and G stars are not necessarily young, and cannot be used as a gauge of today's ISM abundances. Sofia & Meyer (2001), using Edvardsson et al.'s (1993) sample, calculated the average abundances for F and G stars less than 2 Gyr old. They found values for Mg and Si that are similar to the most recent solar values, but less O than solar (Asplund et al. 2009). Some have suggested using abundances measured in H II regions, but this has been rejected due to large systematic errors from temperature fluctuations in the nebula (Mathis 1995; Kingdon & Ferland 1995). Further complicating the situation, and highlighting the need for spectroscopy on nearby objects, is the correlation between Galactocentric distance and abundances (Shaver et al. 1983; Gummersbach et al. 1998; Chiappini et al. 2001), as regions closer to the Galactic center are more metal-rich than outer regions.

A direct measurement of the local ISM is the best way to determine exactly how much material remains for local dust grains. X-ray spectroscopy is particularly useful for this, as the elements that make up the grains have their K- and L- shell absorption edges in this band. The edge depths are dependent on each element's total column density (gas + dust phases). Schattenburg & Canizares (1986) were the first to measure X-ray absorption edges; they used the Einstein Observatory to study the K edges of O and Ne toward the Crab Nebula. Since then, much X-ray spectroscopy has been done, usually toward very bright (and distant) low mass X-ray binaries. Paerels et al. (2001) used the *Chandra X-Ray Observatory*'s LETG to measure the

column densities of O, Ne, and Fe toward 4U 0614+091. Takeji et al. (2002) examined the O edge along the line of sight toward Cyg X-2, and Ueda et al. (2005) determined the abundances of O, Mg, Si, S, and Fe toward GX 13+1, GX 5-1, and GX 340+0. Juett et al. (2004, 2006) examined the K edges of O, Ne, and Fe for several X-ray binaries. Costantini et al. (2012) used *XMM-Newton*, the *International Gamma-Ray Astrophysics Laboratory*, and *Chandra* to study the ISM toward 4U 1820-30, focusing on fitting the Fe L and O K edges with dust constituent spectra derived from experiments. However, these studies used X-ray binaries which, while bright, also had large distances. For instance, 4U 0614+091 is at a distance of 1.5-3.2 kpc (Machin et al. 1990; Paerels et al. 2001; Kuulkers et al. 2010) 4U 1820-30 is located in the globular cluster NGC 6624, between 6.8-9.6 kpc away (Güver et al. 2010). The distance to Cyg X-2 is controversial, with Goranskij & Lyutyj (1988) placing it only 1.6 kpc away, and others (Orosz & Kuulkers 1999; Jonker & Nelemans 2004; Galloway et al. 2008) placing it much farther away, up to ~ 11 kpc. GX 13+1, GX 5-1, and GX 340+0 are near the Galactic center, 7, 9.2, and 11.0 kpc away, respectively (Jonker et al. 2000).

In contrast, X Per is one of the few bright X-ray binaries that is nearby, only $\sim 0.4-1$ kpc distant. Cunningham et al. (2004) used the *Chandra* LETG to examine the line of sight toward X Per and measure the O column density, but the observation unfortunately had low signal-to-noise, leading to an uncertainty of about 50% in their measurement and an inability to impose meaningful constraints on grain models. Thus, to better assess the elemental budget in the nearby ISM, in particular that of silicate-forming dust, and provide insight into possible dust grain compositions, we have obtained and analyzed high-resolution X-ray spectra of X Per from both *Chandra* and *XMM-Newton*.

2. THE X PER SYSTEM

X Persei (HD 24534, BD+30 591) is a Be/X-ray binary and is composed of a neutron star and OB companion of likely spectral type O9.5III to B0V (Liu et al. 2006; Raguzova 2007). It is variable, with $m_V = 6.1-6.8$. The optical variations are believed to be due to the formation and dissipation of an equatorial disk (Telting et al. 1998), similar to other Be binary systems. The neutron star has a rotation period of about 835 s, one of the longest observed for a neutron star (Haberl et al. 1998). Distance estimates from spectroscopic parallax have placed it as far away as 1.3 kpc (e.g., Fabregat et al. 1992) but more recent work indicates that it is closer, at $\sim 0.7-1$ kpc (Lyubimkov et al. 1997; Roche et al. 1997; Telting et al. 1998). Jensen et al. (2005) used spectroscopic parallax to place it at 590 pc, though the most recent reduction of Hipparcos parallaxes places it at 427^{+183}_{-98} pc (van Leeuwen 2007), in agreement with Blaauw's (1952) assessment that it is in the ζ Per OB association ($d = 350$ pc; Johnson 1957). While there is apparently some uncertainty in the distance to X Per, it is nonetheless closer to the Sun than other X-ray binaries that have been used to examine the ISM.

The ISM toward X Per has also been studied extensively, and it happens that this sight line is an excellent representative for the diffuse ISM at large, as seen through the ratio of total-to-selective extinction $R_V (\equiv A_V / (E(B - V)))$. R_V is a general indicator of grain size and local ambient radiation field; it is the sole variable upon which differences in UV extinction curves depend (Cardelli et al. 1989). It ranges from ~ 2.5 (diffuse sight line) to ~ 5.5 (dense sight line), with the "standard diffuse ISM" having $R_V = 3.05 \pm 0.15$ (Whittet 2003); most grain models

assume this standard value. R_V for the X Per line of sight is 3.06 (Valencic & Smith 2008), making X Per ideal for studying the "standard" local ISM.

3. OBSERVATION AND DATA REDUCTION

Two observations were used, one from *Chandra*'s LETG/ACIS-S (ObsID 12447) and the other from *XMM-Newton*'s RGS instrument (ObsID 0600980101). The *Chandra* observation (ObsID 12447) had an exposure time of 131 ks and was reprocessed with CIAO 4.3 (CALDB 4.4.1) according to standard methods for grating spectra as described in the Science Threads⁴ using the task "chandra_repro" to generate a new bad pixel file, event file, and PHA files. Before continuing, the light curve was examined. It did not show any flaring during this time, and displayed only slight variability, with an average count rate of 0.96 ± 0.10 counts s^{-1} . The response and ancillary files for the +1 and -1 orders were then created and applied. The orders were coadded.

The *XMM-Newton* observation (ObsID 0600980101) had an exposure time of 126 ks. It was reprocessed with SAS 11, according to standard procedures described in the "ABC Guide."⁵ The light curve was examined; it showed flaring at the start and end of the observation. Those events were excised, which left an effective exposure time of ~ 100 ks.

The continuum was only measured locally in the RGS and LETG spectra. They were analyzed using Spex⁶ version 2.03.03 (Kaastra et al. 1996). An implementation of the Cash statistic, C-stat, was used (Arnaud et al. 2011). The best fit was determined by finding C-stat/ ν , where $\nu =$ degrees of freedom. The hydrogen column density used throughout, $N_H = (2.20^{+0.18}_{-0.16}) \times 10^{21}$ cm^{-2} , is from Cunningham et al. (2004), who calculated it from the *IUE* and *FUSE* measurements of H I and H₂ from Diplas & Savage (1994) and Rachford et al. (2002), respectively. The column densities of elements in the gas phase, dust phase, and the total column densities are listed in Table 3. The depletions were found as (dust phase abundance/total abundance). The proto-Sun abundances of Lodders (2003) were used as a reference throughout.

3.1. Oxygen

The neutral and lightly ionized gaseous and solid phases of the ISM are expected to comprise the bulk of the ISM along this line of sight, so this study focuses primarily on them. However, heavily and moderately ionized gas may also be present, and the RGS1 spectrum was examined by eye from 18-28 Å to see if there were any features from highly ionized oxygen. Unfortunately, this part of the spectrum contained a chip gap (at 20.75 Å), node boundaries (at 18.91 and 22.72 Å), and bad pixels (at 18.67, 18.96, 19.49, 19.67, 21.81, 22.77, 22.95, and 23.38 Å) which happened to coincide with astrophysically interesting features, such as O II (23.35 Å), O IV (22.73 Å), and O VIII (18.97 Å), and those which pertain to dust, at wavelengths from 22.5-23.2 Å.

Absorption from highly ionized O was not evident. Nonetheless, its absence was tested by fitting the spectrum between 18-28 Å with a lightly absorbed power law with a layer of intervening hot material, as described in the Spex manual.⁷ Spex

⁴ <http://cxc.cfa.harvard.edu/ciao/>

⁵ <http://heasarc.nasa.gov/docs/xmm/abc/>

⁶ <http://www.sron.nl/spex>

⁷ <http://www.sron.nl/spex/manual-hea-menu-1246.html>

Table 1
Dust Compounds Used to Fit the O Edge

Compound	Chemical Formula
Acmite	NaFeSi ₂ O ₆
Almandine	Fe ₃ Al ₂ (SiO ₄) ₃
Andradite	Ca ₃ Fe ₂ Si ₃ O ₁₂
Chromite	FeCr ₂ O ₄
Enstatite	MgSiO ₃
Franklinite	Zn _{0.6} Mn _{0.8} Fe _{1.6} O ₄
Hedenbergite	CaFeSi ₂ O ₆
Hematite	Fe ₂ O ₃
Hercynite	FeAl ₂ O ₄
Ilmenite	FeTiO ₃
Iron oxide	Fe _{1-x} O
Magnetite	Fe ₃ O ₄
Olivine	Mg _{1.6} Fe _{0.4} SiO ₄

allows the user to specify the temperature and velocity dispersion of a modeled gas cloud. The line equivalent widths, and thus the derived column densities, of the ions considered in this work depend somewhat on the velocity broadening; this is discussed in detail in Kaastra et al. (2008). When modeling the contributions from different phases of the ISM, commonly used values of the temperature and velocity dispersion for those phases were used (e.g., Snowden et al. 1997; Sembach et al. 2003; Redfield & Linsky 2004; Savage & Lehnner 2006). First, absorption from cold gas was fit to first order using the component “hot,” which can mimic cold gas when the temperature is set to the component’s minimum allowed value. The temperature and velocity dispersion were held at values typical of cold gas in the ISM, 5×10^{-4} keV and 1 km s^{-1} . The O abundance was allowed to float. The absorption from O VIII was then added, using the “slab” component, which finds the transmission of a thin gas layer. The velocity dispersion was set initially to 150 km s^{-1} , and allowed to float. However, the addition of this slab worsened the fit. The O VIII was replaced with O VII and the spectrum was refit. Again, the fit showed no improvement. The O VII was then replaced with O VI, and the spectrum was refit. Again, the fit showed no improvement. To test for less ionized O, the velocity dispersion was initially set to 100 km s^{-1} and allowed to float; the O VI was swapped out for O V, and the spectrum was fit again using the same procedure; again, there was no improvement in the fit. In light of this, these species were not included in any further models.

The neutral and lightly ionized gas components near 23.5 \AA were considered next, adding one new ISM component at a time, as described the Spex manual. The region from $22.5\text{--}23.2 \text{ \AA}$ was excluded when not fitting O III or dust compounds, as absorption from these components dominate that region and a model that includes that wavelength region without accounting for those absorbing species will not produce a good fit.

As before, the spectrum was fit with a lightly absorbed power law. The absorption from cold gas was again fit using the “hot” component, with the temperature held at the minimum allowed value and the velocity dispersion held at 1 km s^{-1} . The O abundance was allowed to float. The spectrum was examined for O II at 23.35 \AA to see if the feature’s wings might be detectable in the continuum near the cool pixel at 23.38 \AA . A “slab” component was added to the model with the velocity dispersion set to 50 km s^{-1} . This produced an estimate of the O II column density and a C-stat/ ν that was the same as without the slab, but it was included in further fits nonetheless. Next, the region from

Table 2
O Edge Models and Their C-stat/ ν Values

Model	C-stat/ ν
MgSiO ₃ + Mg _{1.6} Fe _{0.4} SiO ₄	873.6/745
MgSiO ₃	876.1/746
MgSiO ₃ + Fe _{1-x} O	875.2/745
Mg _{1.6} Fe _{0.4} SiO ₄	877.4/746
Fe _{1-x} O	877.7/746
Fe ₂ O ₃ + Mg _{1.6} Fe _{0.4} SiO ₄	877.3/745
Fe _{1-x} O + Mg _{1.6} Fe _{0.4} SiO ₄	877.4/745
Fe _{1-x} O + Fe ₂ O ₃	877.7/745
Fe ₂ O ₃	879.0/746
Fe ₃ O ₄	880.2/746

$22.5\text{--}23.2 \text{ \AA}$ was included and O III was added to the model and fitted, producing C-stat/ $\nu = 896.0/749$. Then, O IV was added via the addition of another slab with velocity dispersion set to 100 km s^{-1} ; this improved the C-stat/ ν to $888.2/748$. In all subsequent fits, O I, O II, O III, and O IV were included. Dust was added next, using the Spex component “amol.” All silicon- and iron-bearing dust compounds in the Spex software with laboratory-measured O edge components were tested; these are listed in Table 1. The addition of any type of dust improved the fits over the gas-only model.

A second dust component was added next; all combinations were tried. While the Spex software can accommodate up to four dust compounds, using more than two components tends to drive the column density of one of the other compounds to zero, resulting in effectively a two-compound model. Thus, no more than two compounds were used at a time. Values of C-stat/ ν from models with only one or two types of dust were very similar to each other, often being identical for different models. Models that included complex dust compounds like Ca₃Fe₂Si₃O₁₂, NaFeSi₂O₆, CaFeSi₂O₆, Fe₃Al₂(SiO₄)₃, and FeAl₂O₄ produced poor fits and were removed from consideration. In contrast, models that included FeTiO₃ and Zn_{0.6}Mn_{0.8}Fe_{1.6}O₄ fit the edge very well; however, they also required prohibitively large quantities of Ti and Zn ($>300 A_{\odot}$), so they were not considered further. Models that included Fe₃O₄ and Fe₂O₃ tended to provide worse fits. In particular, Fe₃O₄ had difficulty fitting the edge, as its column density went to 0 in all models that combined it with another dust compound; these models were also excluded from further consideration. The models that remained at this point and their C-stat/ ν are listed in Table 2. Of the models with only one type of dust, MgSiO₃ provided the best fit, followed by Mg_{1.6}Fe_{0.4}SiO₄. Out of all the models that were tested, the best fit was provided by a combination of MgSiO₃ and Mg_{1.6}Fe_{0.4}SiO₄, with $N(\text{MgSiO}_3)/N(\text{Mg}_{1.6}\text{Fe}_{0.4}\text{SiO}_4) = 3.4$. It is shown in Figure 1.

The best fit yielded $\log N(\text{O I}) = 17.88 \pm 0.01$. For comparison, Snow et al. (1998) found $\log N(\text{O I}) = 18.09 \pm 0.06$, and Jensen et al. (2005) found $\log N(\text{O I}) = 17.83^{+0.04}_{-0.03}$ for this line of sight. Meyer et al. (1998) found an average interstellar O I abundance for 13 diffuse lines of sight of $\log N(\text{O I}) = 17.85 \pm 0.02$. Upper limits on O II and O III were found, with $\log N(\text{O II}) < 15.98$ and $\log N(\text{O III}) < 11.38$, respectively, while $\log N(\text{O IV}) = 16.72^{+0.21}_{-0.30}$. The results are listed in Table 3. The depletion, $25\% \pm 3\%$, is similar to what is expected for the diffuse ISM, $\sim 24\%$ (Whittet 2003). The total O abundance, 509^{+48}_{-43} ppm, is within 2σ of the proto-Sun abundances of Lodders (2003), 575.4 ppm.

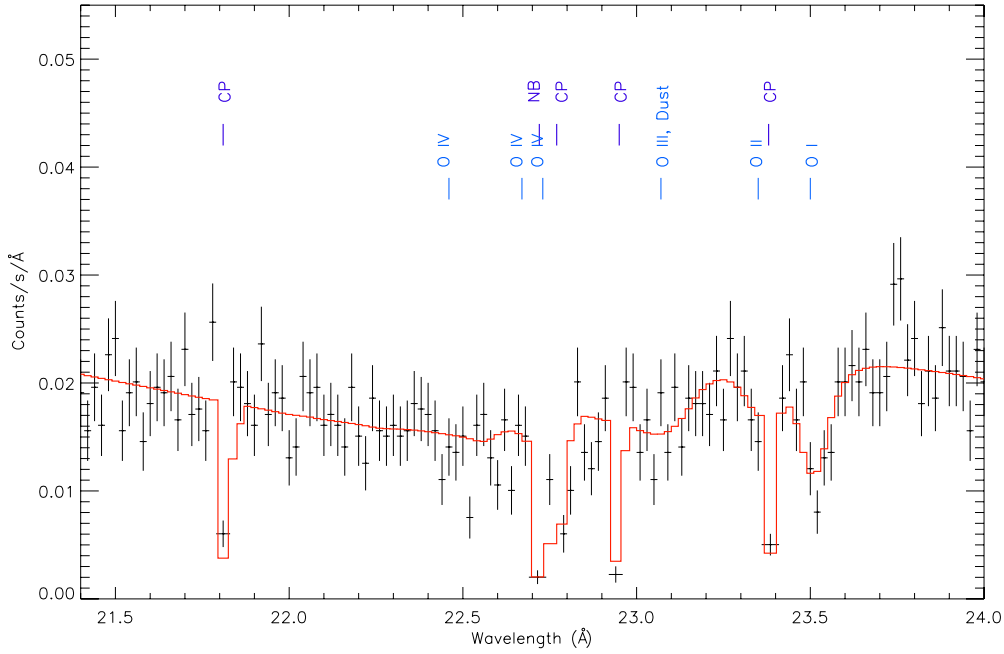


Figure 1. Best fit to the RGS spectrum at the O edge. Cool pixels (“CP”) and a node boundary (“NB”) are indicated. Data have been rebinned for clarity. (A color version of this figure is available in the online journal.)

Table 3
Column Densities and Depletions

Element	$N(X)_{\text{gas}}$ (10^{16} cm^{-2})	$N(X)_{\text{dust}}$ (10^{16} cm^{-2})	$N(X)_{\text{net}}$ (10^{16} cm^{-2})	X/H (ppm)	A/A_{\odot}^a	Depletion (%)
Oxygen	$83.7^{+4.3}_{-3.8}$	28.4 ± 2.6	$112.1^{+5.0}_{-4.6}$	509^{+48}_{-43}	$0.89^{+0.08}_{-0.07}$	25 ± 3
Magnesium	0.26 ± 0.01	6.82 ± 0.65	7.08 ± 0.65	32 ± 4	0.77 ± 0.09	96^{+4}_{-13}
Silicon	$1.05^{+1.80}_{-0.83}$	6.82 ± 0.65	$7.87^{+1.91}_{-1.05}$	36^{+9}_{-5}	$0.88^{+0.22}_{-0.13}$	87^{+13}_{-15}
Iron	$1.29^{+0.38}_{-0.23}$	$6.29^{+0.55}_{-0.31}$	$7.58^{+0.67}_{-0.39}$	34^{+4}_{-3}	$0.99^{+0.12}_{-0.09}$	83^{+10}_{-6}

Note. ^a The proto-Sun abundances of Lodders (2003) are referenced.

Table 4
Dust Compounds Used to Fit the Fe Edge

Compound	Chemical Formula
Fayalite	Fe_2SiO_4
Hematite	Fe_2O_3
Iron monoxide	FeO
Iron sulfate	FeSO_4
Iron sulfite	FeS_2
Lepidocrocite	$\text{FeO}(\text{OH})$
Magnetite	Fe_3O_4
Metallic iron	Fe

3.2. Iron

A similar method was employed at first to examine the Fe L edge in the RGS and LETG spectra. These were fit simultaneously with absorbed power laws, with the Fe abundance allowed to float. In all fits, the Fe absorption terms for each spectrum were linked. A lightly ionized gas was added with the “slab” component, and dust compounds were added with the “amol” component. All compounds with laboratory-measured L edges in Spex were tested, first fitting a single compound, then combinations. The compounds are listed in Table 4. To minimize confusion, $N(\text{Fe II})$ was held at the value found by Jensen & Snow (2007).

Spex includes laboratory measurements of the O and Fe edges of both Fe_3O_4 and Fe_2O_3 which allows for cross-checks between results of fits to the two edges. The results from fitting the Fe edge with these compounds are similar to that of the O edge, with Fe_2O_3 consistently providing worse fits than other compounds. In contrast, Fe_3O_4 could provide good fits in combination with other compounds, particularly metallic Fe. To test this, the O edge was re-fit with a combination of Fe_3O_4 (held at the value from the Fe fit) and MgSiO_3 . This produced $C\text{-stat}/\nu = 879.8/746$, worse than the $(\text{MgSiO}_3 + \text{Mg}_{1.6}\text{Fe}_{0.4}\text{SiO}_4)$ fit ($\Delta C\text{-stat} = 6.2$), but MgSiO_3 and O I column densities were within 3σ of those found using the $(\text{MgSiO}_3 + \text{Mg}_{1.6}\text{Fe}_{0.4}\text{SiO}_4)$ combination.

Some models that used sulfurous compounds provided good fits. However, some of these also required $2.8\text{--}4.3 A_{\odot}$: (metallic Fe + FeS_2), $(\text{Fe}_2\text{SiO}_4 + \text{FeS}_2)$, and $(\text{FeSO}_4 + \text{FeS}_2)$. To test if these overabundances would be measurable in the spectrum, simulated spectra were made and fitted. The spectra were constructed using an absorbed power law as the continuum with the S abundance set to $2.8 A_{\odot}$ and $4.3 A_{\odot}$. The S K edge is at 5.01 \AA , and the spectra were examined from $3\text{--}7 \text{ \AA}$. In both cases, the overabundance was recovered, with values of 2.5 ± 0.9 and $5.9 \pm 1.0 A_{\odot}$, respectively. Then, the real spectrum was also examined over the same range and with the same model; no overabundance was detected.

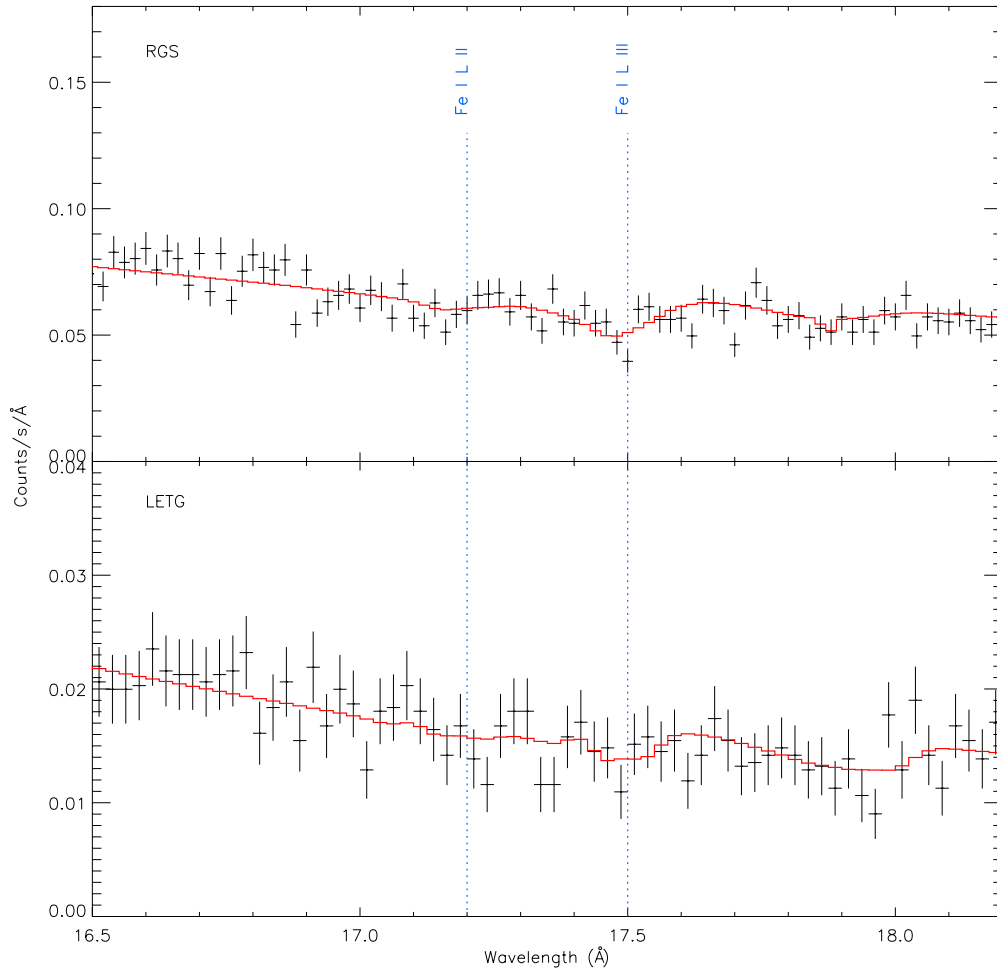


Figure 2. Best fit to the RGS and LETG spectra at the Fe edge. Data have been rebinned for clarity. (A color version of this figure is available in the online journal.)

In some of the models with two dust components, one of the components dominated and the other component went to 0; this tended to happen in combinations with metallic Fe as this compound tended to be strongly favored. These two-dust component models (which were effectively one-dust component models) were also removed. The models that remained and their $C\text{-stat}/\nu$ values are listed in Table 5. Of the models with one dust compound, metallic Fe fared best, and the models with two dust components also favored it. As with the O edge, the fits tended to favor simpler compounds (such as metallic Fe) over more complex ones (such as $\text{FeO}(\text{OH})$). The fits also tended to have extremely similar $C\text{-stat}/\nu$, with the two best models, (metallic Fe + FeO) and (metallic Fe + Fe_3O_4), having identical $C\text{-stat}/\nu$. The fit to (metallic Fe + Fe_3O_4) is shown in Figure 2. The ratios of dust compounds in the best two-dust models were $N(\text{metallic Fe})/N(\text{FeO}) = 0.8$, and $N(\text{metallic Fe})/N(\text{Fe}_3\text{O}_4) = 2.4$.

However, while these produced the best fits, they were not particularly “good” fits, as a careful examination of the spectrum near 17.7 \AA shows a mismatch between the model and data, with higher flux than the model can account for. This can also be seen in the data presented by Kaastra et al. (2009), Pinto et al. (2010), and Costantini et al. (2012) in their analyses of the Crab Nebula, GS 1826–238, and 4U 1820–30, respectively. Further, near the L II edge, there appears to be more absorption at 17.1 \AA and an excess of flux at 17.2 \AA than accounted for in the best fit.

Table 5
Fe Edge Dust Models and Their $C\text{-stat}/\nu$ Values

Model	$C\text{-stat}/\nu$
Metallic Fe + FeO	947.0/879
Metallic Fe + Fe_3O_4	947.0/879
$\text{FeO} + \text{Fe}_2\text{SiO}_4$	947.7/879
$\text{FeO} + \text{FeO}(\text{OH})$	948.5/879
$\text{Fe}_3\text{O}_4 + \text{FeO}(\text{OH})$	948.8/879
$\text{FeSO}_4 + \text{FeO}$	949.6/879
$\text{Fe}_3\text{O}_4 + \text{Fe}_2\text{O}_3$	949.6/879
$\text{Fe}_3\text{O}_4 + \text{FeSO}_4$	949.7/879
$\text{FeO} + \text{Fe}_2\text{O}_3$	949.7/879
Metallic Fe	954.4/880
Fe_3O_4	955.1/880
$\text{FeO} + \text{FeS}_2$	955.1/879
Fe_2O_3	962.2/880
$\text{FeO}(\text{OH})$	962.7/880
Fe_2SiO_4	962.7/880
Fe_3O_4	965.2/880

Unfortunately, Spex does not include a laboratory measurement of $\text{Mg}_{1.6}\text{Fe}_{0.4}\text{SiO}_4$ at the Fe L edge, so this compound cannot be tested. Both best fit models produced a high Fe abundance, $53 \pm 5 \text{ ppm}$, or $1.5 \pm 0.1 A_{\odot}$. While Fe may indeed be overabundant along this sightline, the mismatches between the

fit and the data make this conclusion uncertain, as does the fact that the model that used metallic Fe alone produced only a slightly worse C-stat/ ν and a far lower Fe abundance, 34^{+4}_{-3} ppm ($99^{+12}_{-9}\%$ A_{\odot}). This value is listed in Table 3. The Fe depletion is often considered to be near 100% (Savage & Sembach 1996; Whittet 2003); the value found in this work, $83^{+10}_{-6}\%$, is notably lower but in agreement with that given by Wilms et al. (2000), 70%.

3.3. Silicon

As with the O and Fe edges, several absorbers are expected to be present at the Si K edge. The LETG spectrum was fitted from 5–10 Å with an absorbed power law, with the Si abundance allowed to float. As before, models were built up piece by piece, with lightly ionized gas being added through the “slab” component, and dust compounds were added with the “amol” component. All compounds with laboratory-measured Si K edges in Spex were tested, first fitting a single compound, then combinations. To minimize confusion between absorption from different components, values for $N(\text{Si II})$ and $N(\text{Si IV})$ were set to those measured using UV absorption lines (Gnacinski & Krogulec 2006; Savage et al. 2001) and the edge was refit. However, fits produced unrealistic column densities, so the column density of MgSiO_3 , which has laboratory-measured spectra at both the O K and Si K edges, was then set to the result of the O fit, and the edge was refit again. This yielded upper limits on Si I and Si III: $\log N(\text{Si I}) < 15.91$ and $\log N(\text{Si III}) < 9.98$. The total Si abundance was then 36^{+9}_{-5} ppm, or $88^{+22}_{-15}\%$ A_{\odot} . The results are listed in Table 3. The depletion, $87^{+13}_{-15}\%$, is lower than expected from other measurements of the diffuse ISM (Wilms et al. 2000: 90%; Whittet 2003: 96%) but is nonetheless consistent within 1σ .

3.4. Magnesium

The LETG data was examined, as the detector does not have internal Mg features, unlike RGS. Unfortunately, Spex does not currently include any compounds with laboratory-measured Mg K edges. Therefore, the Mg edge in the LETG spectrum was fitted from 9–10 Å with a gas-only model. As usual, the model was built up one component at a time, starting with a lightly absorbed power law. Values for $N(\text{Mg I})$ and $N(\text{Mg II})$ were held at those measured using UV absorption lines (Gnacinski & Krogulec (2006)). This yielded an upper limit for $\log N(\text{Mg III}) < 14.05$. The column density of MgSiO_3 from the O edge fit was again used to calculate the amount of Mg in grains, so the total Mg abundance was 32 ± 4 ppm, or $77\% \pm 9\%$ A_{\odot} , which was notably less than the proto-Sun Mg abundance of Lodders (2003), but was nonetheless within 3σ of it. The depletion, $96^{+4}_{-13}\%$, is higher than expected from the diffuse ISM (87%; Whittet 2003) though the large uncertainty allows it to be within 1σ . The results are listed in Table 3.

4. DISCUSSION

4.1. Dust Compounds

The O edge fit shows MgSiO_3 is likely a major contributor to the absorption there, possibly in combination with olivine, $\text{Mg}_{1.6}\text{Fe}_{0.4}\text{SiO}_4$. The edge’s ability to be fit with MgSiO_3 has also been observed along the sightline to 4U 1820–30 by Costantini et al. (2012). They also found that compounds containing oxygen and iron together (such as Fe_3O_4 and Fe_2O_3) worsened their fits to the point where they were able to rule

them out. Similarly, the O edge fit in this study shows that these compounds are not likely to be major contributors to the O K edge in this line of sight. However, Costantini et al. (2012) also found that iron-bearing silicates such as $\text{Mg}_{1.6}\text{Fe}_{0.4}\text{SiO}_4$ were not likely to be major absorbers for their sightline; in contrast, while the X Per sightline favors MgSiO_3 , it also produces a better fit when iron-bearing silicate is included. Silicates have long been known to be major constituents of the ISM. The Si–O stretching and bending bonds of amorphous silicate have been observed at 10 and 18.5 μm along the heavily extinguished sightlines toward the Galactic center (Roche & Aitken 1985) and along sightlines in the diffuse ISM, as well as toward dense molecular clouds (van Breemen et al. 2011). This has often been attributed to some combination of MgSiO_3 and $(\text{Mg}, \text{Fe})_2\text{SiO}_4$ (e.g., Kemper et al. 2004; Chiar & Tielens 2006; Min et al. 2007). Work by Min et al. (2007) suggested that extinction toward the Galactic center at 10 μm is well modeled with a combination of about 85% MgSiO_3 and 15% $(\text{Mg}, \text{Fe})_2\text{SiO}_4$. Similarly, the sightline to X Per suggests that $77 \pm 10\%$ is MgSiO_3 and $23\% \pm 5\%$ is in $\text{Mg}_{1.6}\text{Fe}_{0.4}\text{SiO}_4$, which, despite having slightly different stoichiometry, agrees with Min et al.’s (2007) result within the uncertainty.

The best fits to the Fe L edge were produced by combinations of (metallic Fe + FeO) and (metallic Fe + Fe_3O_4). This is similar to Costantini et al.’s (2012) finding that metallic Fe could well fit the absorption along the line of sight to 4U 1820–30. In the present study, Fe_2O_3 did not provide good fits at either the O or Fe edges; this too agrees with the findings of Costantini et al. (2012). The apparent prevalence of metallic Fe in the diffuse ISM is not expected. Iron in the ISM has long been thought to be primarily in oxides, sulfurous compounds, and olivines (Jones 1990; Savage & Sembach 1996). This is due in part to observations of the ISM itself and dust-producing stars, and partly from expected lifetimes of dust grains. As noted earlier, studies of silicate grains in the ISM have pointed to the presence of a combination of Mg-rich- and Fe-bearing silicates (Spitzer & Fitzpatrick 1993, 1995; Kemper et al. 2000, 2004; Min et al. 2007). Further, a study of pre-solar grains in meteorites has also identified Fe-bearing silicates (Bose et al. 2010).

Studies of the dust shells around O-rich asymptotic giant branch (AGB) stars, where one would expect to find silicate dust compounds prior to their flowing into the ISM, have typically found that most of the Fe is in amorphous (and possibly crystalline; Guha Niyogi et al. 2011) olivines, possibly with a small amount in iron oxides (Molster et al. 1999; Demyk et al. 2000), though Kemper et al. (2002) found that the addition of a small amount of metallic Fe improved their fit to IR extinction in an AGB star’s dust shell.

The type of dust that forms in AGB star winds depends on the star’s metallicity and the pressure and temperature of the stellar wind (Speck 2012 and references therein). Gail & Sedlmayr (1999) modeled the formation of grains around an M star and showed that Fe vapor could condense at slightly cooler temperatures than silicates, and thus precipitate on the silicate grains. It was unclear, however, if these precipitates remained on the grains, and were eventually covered with more silicate (thus forming inclusions), or if they left the surface, either through collisions with other grains or mechanical stresses with the substrate in the case of irregular grain growth (thus forming metallic grains; Gail & Sedlmayr 1999).

However, any metallic Fe grains that formed in a stellar wind and were injected into the ISM would oxidize quickly, as small grains ($\sim 0.01 \mu\text{m}$) react with the O-rich diffuse ISM to form

Table 6
Abundances toward X Per and Some Other X-Ray Binaries

Object	l ($^{\circ}$)	b ($^{\circ}$)	Distance (kpc)	Distance Reference	O/H (ppm)	Abundance Reference
Cyg X-2	87.3	-11.3	>1.6	(1), (2), (3), (4)	478 ± 135	(12)
4U 1636-53	332.9	-4.8	6 ± 0.5	(2)	491^{+270}_{-88}	(12)
4U 1820-30	2.8	-7.9	6.4 ± 0.2	(2)	485^{+102}_{-78}	(12)
4U 1735-44	346.1	-7.0	8.5 ± 1.3	(2)	486 ± 22	(12)
GX 9+9	8.5	9.0	5 ± 1	(5)	489^{+372}_{-186}	(12)
4U 1543-624	321.8	-6.3	7.5 ± 0.5	(6)	467^{+560}_{-252}	(12)
Cyg X-1	71.3	3.1	$2^{+0.4}_{-0.3}$	(7)	492 ± 64	(12)
4U 0614+091	200.9	-3.4	$2.2^{+0.8}_{-0.7}$	(8), (9), (10)	533	(10)
X Per	163.1	-17.1	$0.43^{+0.18}_{-0.10}$	(11)	509^{+48}_{-43}	This work

References. (1) Goranskij & Lyutyj 1988; (2) Galloway et al. 2008; (3) Orosz & Kuulkers 1999; (4) Jonker & Nelemans 2004; (5) Christian & Swank 1997; (6) Jonker et al. 2000; (7) Ziółkowski 2005; (8) Machin et al. 1990; (9) Kuulkers et al. 2010; (10) Paerels et al. 2001; (11) van Leeuwen 2007; (12) Juett et al. 2004.

sulfates and oxides in only ~ 1 Myr; larger grains ($\sim 0.1 \mu\text{m}$) react slightly less quickly but still only require ~ 10 Myr, still well within the lifetime of a typical diffuse cloud, ~ 10 – 100 Myr (Jones 1990). Further, models of interstellar shocks, such as those from supernovae and cloud collisions, suggest that pure metallic Fe grains are destroyed more quickly than oxides, making metallic Fe grains unlikely to survive in the ISM (Savage & Sembach 1996).

This lends itself to the suggestion that metallic Fe inclusions in silicates, or glass with embedded metal and sulfides (GEMS) might contribute to Fe L edge absorption. GEMS have been studied in interplanetary dust particles, and while the overwhelming majority (94%–99%) have solar system origins, the remaining very small fraction (1%–6%) may be minimally processed circumstellar material that survived its passage in the ISM and subsequent incorporation into the solar nebula (Keller & Messenger 2011). If GEMS are a major ISM dust population, they should be detectable at other wavelengths. Draine & Lazarian (1999) showed that metallic Fe is expected to produce strong emission at 70–90 GHz. This emission was not observed, and they estimated that $\leq 5\%$ of Fe in dust grains can be in metallic form, either as grains or inclusions in GEMS. However, a more recent analysis of the magnetic properties of metal grains and oxides (Draine & Hensley 2013) disputes this, and shows that a substantial amount of the Fe in the ISM may be in oxides or metals without violating the observed emission constraints.

Thus, if the identification of metallic Fe is correct, it may be that much of the Fe in the ISM along the sightline to X Per is in the form of inclusions in silicates. However, it is worth recalling the difficulty the models had fitting the feature, and, as noted before, $\text{Mg}_{1.6}\text{Fe}_{0.4}\text{SiO}_4$ cannot currently be tested at the Fe L edge; the only Fe-bearing silicate with a laboratory measurement at the Fe L edge that is included in Spex is Fe_2SiO_4 . It may be worth noting that the model that included (FeO + Fe_2SiO_4) produced the third-best C-stat/ ν after the (metallic Fe + FeO) and (metallic Fe + Fe_3O_4) In any case, this highlights the need for more laboratory measurements of Fe-bearing dust compounds at X-ray energies.

4.2. Abundances Compared to Other Measurements

The abundances found here strongly depend on the dust compounds that were used in the model. While the identity of the absorber(s) at the Fe L edge is not clear, the identifications

at the other edges is more solid, so some insight might be gained by comparing the O, Mg, and Si abundances to reference measurements. The abundances found here are within 3σ of those of the proto-Sun estimates of Lodders (2003), with O at 1.4σ , Mg at 2.5σ , and Si at 1.2σ . There are comparable levels of agreement between them and young F and G stars (Sofia & Meyer 2001), with O at 1.5σ , Mg at 2.7σ , and Si at 1σ . However, the abundances for Mg and Si are notably less than either reference. They are in better agreement with the most recent B star abundances of Simón-Díaz (2010) and Nieva & Simón-Díaz (2011), with O at 0.6σ , Mg at 1.3σ , and Si at 0.9σ . In those studies, they determined the stellar parameters and elemental abundances of a sample of nearby B stars from spectroscopic analyses using the same set of stellar atmosphere models. This contrasts with earlier studies, which relied on photometric analysis to determine stellar parameters, and then performed the spectroscopic abundance analysis. These recent works led to higher abundances than previously reported for these same stars, which brought them closer to, though not necessarily in agreement with, proto-Sun values (Lodders 2003). The results found in the present work lend support to these re-analyzed B stars as indicators of current local ISM abundances.

4.3. Abundances Compared to Other X-Ray Binaries

The O abundance results from this work were also compared to O measurements toward some other X-ray binaries along diffuse lines of sight in order to gauge how the O abundance changes with distance from the Galactic center. These can be seen in Table 6. Paerels et al. (2001) examined the line of sight toward 4U 0614+091, a relatively nearby source which is located almost directly opposite the Galactic center. Juett et al. (2004) studied seven lines of sight toward bright, distant X-ray binaries. The nearest may be Cyg X-2, with distance measurements ranging from ~ 1.6 – 11 kpc (Goranskij & Lyutyj 1988; Orosz & Kuulkers 1999; Jonker & Nelemans 2004; Galloway et al. 2008); if so, the next nearest is Cyg X-1, is at a distance of ~ 2 kpc (Ziółkowski 2005). Juett et al. (2004) fitted the O K edges with neutral and ionized gas and fixed N_{H} to be consistent with the O measurement, assuming the O abundance of Wilms et al. (2000). However, measurements of elemental abundances toward B stars, H II regions, and planetary nebulae have shown that they diminish with distance from the Galactic center (Chiappini et al. 2001 and references therein),

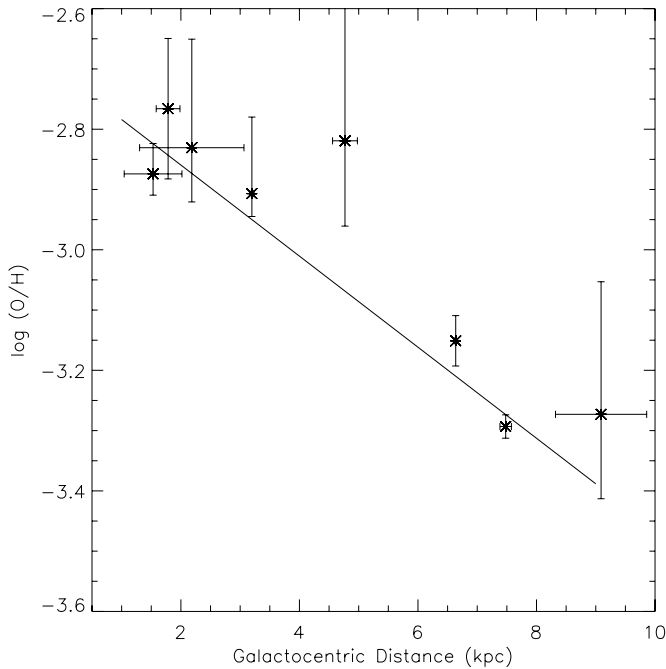


Figure 3. O abundance plotted against Galactocentric distance for a sample of X-ray binaries. The solid line indicates the best fit.

so Wilms et al.’s (2000) estimate of the ISM abundances may not apply to these sightlines. So, another estimate of N_{H} was found and the O abundances recalculated. Neutral H is the dominant species of H in the diffuse ISM (Takei et al. 2002) so N_{H} was estimated by finding the H I column density within 1° of each of the sources using the weighted average from the H I survey of Kalberla et al. (2005). Because Juett et al. (2004) considered only the gas component, the total O column densities for sources they examined was found by assuming Whittet’s (2003) depletion for the diffuse ISM, 24%.

The distances to the absorbing material was considered next. The disk of the Galaxy has a scale height of about 750 ± 70 pc (de Jong et al. 2010), so most of these objects are within the disk; the Galactocentric distances for these objects were found. However, two sources were not in the disk: 4U 1820–30, which is in the globular cluster NGC 6624, and 4U 1735–44, which have distances below the plane of 1050 pc and 1040 pc, respectively. Most of the intervening material along these lines of sight is likely to be confined to the disk. If there is no absorbing material beyond the thick disk, the distance to the edge of the absorbing material toward 4U 1820–30 is 5.5 kpc and for 4U 1735–44 it is 6.2 kpc. These “absorber distances” were used to find the Galactocentric distances for these two objects. The new O abundances and Galactocentric distances are plotted in Figure 3. Cyg X-2 was not included, due to the large uncertainty in its distance. The best fit line shows a reduction of O abundance with a distance from the Galactic center of -0.076 ± 0.006 dex kpc^{-1} . For comparison, the gradient found with H II regions, B stars, and planetary nebulae ranges from ~ -0.04 to -0.07 dex kpc^{-1} (Afflerbach et al. 1997; Gummersbach et al. 1998; Maciel & Quireza 1999; Deharveng et al. 2000; Rudolph et al. 2006), though Pottasch & Bernard-Salas (2006) found a steeper gradient of -0.085 dex kpc^{-1} . Oxygen is not the only element to show a correlation between abundance and Galactocentric distance; studies of abundances in the Galaxy indicate that other dust-forming elements follow the same trend, albeit with different rates of diminishment

(Chiappini et al. 2001 and references therein; Rudolph et al. 2006). This suggests that the ISM abundances that are derived from absorption spectra of X-ray binaries follow similar trends with Galactocentric distance as those seen in other objects, which highlights the importance of selecting nearby X-ray binaries in studies of the local ISM.

5. CONCLUSIONS

The elemental abundances and dust grains along the line of sight toward X Per were examined by modeling the O K, Mg K, Si K, and Fe L edges in spectra obtained with the *Chandra* and *XMM-Newton* X-ray observatories. The results are summarized as follows.

1. The O K edge was well fit with models that contained MgSiO_3 , with the best fit being provided by a combination of MgSiO_3 and $\text{Mg}_{1.6}\text{Fe}_{0.4}\text{SiO}_4$. In that model, MgSiO_3 was favored, with $N(\text{MgSiO}_3)/N(\text{Mg}_{1.6}\text{Fe}_{0.4}\text{SiO}_4) \sim 3$. This is similar to results from other studies of the ISM, which indicate that silicate dust is primarily Mg-rich, with some Fe-bearing silicates.
2. The best fits to the Fe L edge were provided by models that included metallic iron. However, there were discrepancies between the fits and data, and the exact nature of the absorbers there are not well described by the laboratory spectra currently available. An equally good fit was found by combining oxide with Fe-rich silicate. More laboratory-measured dust analogs are needed for better identification of the absorber.
3. The total abundances of O, Mg, and Si were in better agreement with those of recently re-analyzed B stars than the proto-Sun or young F and G stars, suggesting that they may be better indicators of abundances in the ISM. The depletions of these same elements were consistent within 1σ of the diffuse ISM depletions of Whittet (2003).
4. The O abundances derived from X-ray binary absorption spectra show a correlation with Galactocentric distances, in agreement with what has been seen toward other sources (e.g., H II regions, planetary nebulae), with the O abundance diminishing 0.076 ± 0.006 dex kpc^{-1} . As other dust-forming elements show a similar correlation in these other sources, this emphasizes the need for selecting nearby objects when examining the local ISM.

The authors are grateful to an anonymous referee, whose thoughtful comments improved this work. This work was supported by *Chandra* Award No. GO1-12052A.

Facilities: CXO (ACIS), XMM (RGS)

REFERENCES

- Afflerbach, A., Churchwell, E., & Werner, M. W. 1997, *ApJ*, **478**, 190
 Anders, E., & Grevesse, N. 1989, *GeCoA*, **53**, 197
 Arnaud, K., Smith, R., & Siemiginowska, A. (ed.) 2011, *Handbook of X-ray Astronomy* (1st ed.; Cambridge: Cambridge Univ. Press)
 Asplund, M., Grevesse, N., & Sauval, M. 2005, in *ASP Conf. Ser. 336, Cosmic Abundances as Records of Stellar Evolution and Nucleosynthesis in Honor of David L. Lambert*, ed. T. G. Barnes III & F. N. Bash (San Francisco, CA: ASP), 25
 Asplund, M., Grevesse, N., Sauval, A. J., & Scott, P. 2009, *ARA&A*, **47**, 481
 Blaauw, A. 1952, *BAN*, **11**, 405
 Bose, M., Floss, C., & Stadermann, F. J. 2010, *ApJ*, **714**, 1624
 Cardelli, J. A., Clayton, G. C., & Mathis, J. S. 1989, *ApJ*, **345**, 245
 Cardelli, J. A., & Meyer, D. M. 1997, *ApJL*, **477**, L57
 Cardelli, J. A., Meyer, D. M., Jura, M., & Savage, B. D. 1996, *ApJ*, **467**, 334
 Chiappini, C., Matteucci, F., & Romano, D. 2001, *ApJ*, **554**, 1044

- Chiar, J. E., & Tielens, A. G. G. M. 2006, *ApJ*, **637**, 774
- Christian, D. J., & Swank, J. H. 1997, *ApJS*, **109**, 177
- Costantini, E., Pinto, C., Kaastra, J. S., et al. 2012, *A&A*, **539**, 32
- Cunningham, N. J., McCray, R., & Snow, T. P. 2004, *ApJ*, **611**, 353
- de Jong, J. T. A., Yanny, B., Rix, H.-W., et al. 2010, *ApJ*, **714**, 663
- Deharveng, L., Peña, M., Caplan, J., & Costero, R. 2000, *MNRAS*, **311**, 329
- Demyk, K., Dartois, E., Wiesemeyer, H., Jones, A. P., & d'Hendecourt, L. 2000, *A&A*, **364**, 170
- Diplas, A., & Savage, B. D. 1994, *ApJS*, **93**, 211
- Draine, B. T., & Hensley, B. 2013, *ApJ*, **765**, 159
- Draine, B. T., & Lazarian, A. 1999, *ApJ*, **512**, 740
- Edvardsson, B., Andersen, J., Gustafsson, B., et al. 1993, *A&AS*, **275**, 101
- Fabregat, J., Reglero, V., Coe, M. J., et al. 1992, *A&A*, **259**, 522
- Gail, H.-P., & Sedlmayr, E. 1999, *A&A*, **347**, 594
- Galloway, D. K., Muno, M. P., Hartman, J. M., et al. 2008, *ApJS*, **179**, 360
- Gnacinski, P., & Krogulec, M. 2006, *AcA*, **56**, 373
- Goranskij, V. P., & Lyutyj, V. M. 1988, *SvA*, **32**, 193
- Grevesse, N., & Sauval, A. J. 1998, *SSRv*, **85**, 161
- Guha Niyogi, S., Speck, A. K., & Onaka, T. 2011, *ApJ*, **733**, 93
- Gummersbach, C. A., Kaufer, A., Schaefer, D. R., et al. 1998, *A&A*, **338**, 881
- Güver, T., Wroblewski, P., Camarota, L., & Özel, F. 2010, *ApJ*, **719**, 1807
- Haberl, F., Angelini, L., Motch, C., & White, N. E. 1998, *A&A*, **330**, 189
- Hempel, M., & Holweger, H. 2003, *A&A*, **408**, 1065
- Jensen, A. G., Rachford, B. L., & Snow, T. P. 2005, *ApJ*, **619**, 891
- Jensen, A. G., & Snow, T. P. 2007, *ApJ*, **669**, 378
- Johnson, H. L. 1957, *ApJ*, **126**, 121
- Jones, A. P. 1990, *MNRAS*, **245**, 331
- Jonker, P. G., Fender, R. P., Hambly, N. C., & van der Klis, M. 2000, *MNRAS*, **315**, L57
- Jonker, P. G., & Nelemans, G. 2004, *MNRAS*, **354**, 355
- Juett, A. M., Schulz, N. S., & Chakrabarty, D. 2004, *ApJ*, **612**, 308
- Juett, A. M., Schulz, N. S., Chakrabarty, D., & Gorczyca, T. W. 2006, *ApJ*, **648**, 1066
- Kaastra, J. S., de Vries, C. P., Costantini, E., & den Herder, J. W. A. 2009, *A&A*, **497**, 291
- Kaastra, J. S., Mewe, R., & Nieuwenhuijzen, H. 1996, in 11th Colloquium on UV and X-ray Spectroscopy of Astrophysical and Laboratory Plasmas, ed. K. Yamashita & T. Watanabe (Tokyo: Universal Academy Press), 411
- Kaastra, J. S., Paerels, F. B. S., Durret, F., Schindler, S., & Richter, P. 2008, *SSRv*, **134**, 155
- Kalberla, P. M. W., Burton, W. B., Hartmann, D., et al. 2005, *A&A*, **440**, 775
- Keller, L., & Messenger, S. 2011, *GeCoA*, **75**, 5336
- Kemper, F., de Koter, A., Waters, L. B. F. M., Bouwman, J., & Tielens, A. G. G. M. 2002, *A&A*, **384**, 585
- Kemper, F., Sylvester, R. J., Barlow, M. J., et al. 2000, in ASP Conf. Ser. 196, Thermal Emission Spectroscopy and Analysis of Dust, Disks, and Regoliths, ed. M. R. Sitko, A. L. Sprague, & D. K. Lynch (San Francisco, CA: ASP), 15
- Kemper, F., Vriend, W. J., & Tielens, A. G. G. M. 2004, *ApJ*, **609**, 826
- Kingdon, J. B., & Ferland, G. J. 1995, *ApJ*, **450**, 691
- Kuulkers, E., in 't Zand, J. J. M., Atteia, J.-L., et al. 2010, *A&A*, **514**, 65
- Liu, Q. Z., van Paradijs, J., & van den Heuvel, E. P. J. 2006, *A&A*, **455**, 1165
- Lodders, K. 2003, *ApJ*, **591**, 1220
- Lodders, K., Palme, H., & Gail, H.-P. 2009, in Landolt-Börnstein, New Series, Vol. VI/4B, ed. J. E. Trümper (Berlin: Springer), 560
- Lyubimkov, L. S., Rostopchin, S. I., Roche, P., & Tarasov, A. E. 1997, *MNRAS*, **286**, 549
- Machin, G., Callanan, P. J., Charles, P. A., et al. 1990, *MNRAS*, **247**, 205
- Maciel, W. J., & Quireza, C. 1999, *A&A*, **345**, 629
- Mathis, J. S. 1995, *RMxAA*, **3**, 207
- Meyer, D. M., Jura, M., & Cardelli, J. 1998, *ApJ*, **493**, 222
- Min, M., Waters, L. B. F. M., de Koter, A., et al. 2007, *A&A*, **462**, 667
- Molster, F. J., Waters, L. B. F. M., Trams, N. R., et al. 1999, *A&A*, **350**, 163
- Nieva, M.-F., & Simón-Díaz, S. 2011, *A&A*, **532**, 2
- Orosz, J., & Kuulkers, E. 1999, *MNRAS*, **305**, 132
- Paerels, F., Brinkman, A. C., van der Meer, R. L. J., et al. 2001, *ApJ*, **546**, 338
- Pinto, C., Kaastra, J. S., Costantini, E., & Verbunt, F. 2010, *A&A*, **521**, 79
- Pottasch, S. R., & Bernard-Salas, J. 2006, *A&A*, **457**, 189
- Rachford, B. L., Snow, T. P., Tumlinson, J., et al. 2002, *ApJ*, **577**, 221
- Raguzova, N. V. 2007, *BeSN*, **38**, 24
- Redfield, S., & Linsky, J. L. 2004, *ApJ*, **613**, 1004
- Roche, P., Larionov, V., Tarasov, A. E., et al. 1997, *A&A*, **322**, 139
- Roche, P. F., & Aitken, D. K. 1985, *MNRAS*, **215**, 425
- Rudolph, A. L., Fich, M., Bell, G. R., et al. 2006, *ApJS*, **162**, 346
- Savage, B. D., & Lehner, N. 2006, *ApJS*, **162**, 134
- Savage, B. D., Meade, M. R., & Sembach, K. R. 2001, *ApJS*, **136**, 631
- Savage, B. D., & Sembach, K. R. 1996, *ARA&A*, **34**, 279
- Sembach, K. R., Wakker, B. P., Savage, B. D., et al. 2003, *ApJS*, **146**, 165
- Schattenburg, M. L., & Canizares, C. R. 1986, *ApJ*, **301**, 759
- Shaver, P. A., McGee, R. X., Newton, L. M., Danks, A. C., & Pottasch, S. R. 1983, *MNRAS*, **204**, 53
- Simón-Díaz, S. 2010, *A&A*, **510**, 22
- Snow, T. P., Hansen, M. M., Black, J. H., et al. 1998, *ApJL*, **504**, L55
- Snowden, S. L., Egger, R., Freyberg, M. J., et al. 1997, *ApJ*, **485**, 125
- Sofia, U. J., Cardelli, J. A., Guerin, K. P., et al. 1997, *ApJL*, **482**, L105
- Sofia, U. J., Fitzpatrick, E., & Meyer, D. M. 1998, *ApJL*, **504**, L47
- Sofia, U. J., & Meyer, D. M. 2001, *ApJL*, **554**, L221
- Speck, A. K. 2012, *JAVSO*, **40**, 244
- Spitzer, L., & Fitzpatrick, E. L. 1993, *ApJ*, **409**, 299
- Spitzer, L., & Fitzpatrick, E. L. 1995, *ApJ*, **445**, 196
- Takei, Y., Fujimoto, R., Mitsuda, K., & Onaka, T. 2002, *ApJ*, **581**, 307
- Telting, J. H., Waters, L. B. F. M., Roche, P., et al. 1998, *MNRAS*, **296**, 785
- Ueda, Y., Mitsuda, K., Murakami, H., & Matsushita, K. 2005, *ApJ*, **620**, 274
- Valencic, L. A., & Smith, R. K. 2008, *ApJ*, **672**, 984
- van Breemen, J. M., Min, M., Chiar, J. E., et al. 2011, *A&A*, **526**, A152
- van Leeuwen, F. 2007, *A&A*, **474**, 653
- Whittet, D. C. B. 2003, *Dust in the Galactic Environment* (Bristol: Institute of Physics Publishing)
- Wilms, J., Allen, A., & McCray, R. 2000, *ApJ*, **542**, 914
- Ziółkowski, J. 2005, *MNRAS*, **358**, 851